coatings

MDPI

Article

Pyrrol-Anthracene: Synthesis, Characterization and Its Application as Active Material in Humidity, Temperature and Light Sensors

Muhammad Zeb [1], Muhammad Tahir [1,*], Fida Muhammad [1], Zahid Gul [1], Fazal Wahab [2], Mahidur R. Sarker [3,*], Mohamad Hanif Md Saad [3], Alamgeer [1], Shabina Ali [1], Syed Zafar Ilyas [4] and Salman Ali [5]

[1] Department of Physics, Faculty of Physical and Numerical Sciences, Abdul Wali Khan University Mardan, Mardan 23200, Pakistan; mzebphy@gmail.com (M.Z.); fida_physics@hotmail.com (F.M.); zahidgulecp@gmail.com (Z.G.); alamgeer.phy@awkum.edu.pk (A.); sadozaispogmay@gmail.com (S.A.)
[2] Department of Physics, Karakoram International University, Giligit 15100, Pakistan; fazal.wahab@kiu.edu.pk
[3] Institute of IR 4.0, Unverisity Kebangsaan Malaysia, Bangi 43600, Malaysia; hanifsaad@ukm.edu.my
[4] Department of Physics, Allama Iqbal Open University (AIOU), Islamabad 44000, Pakistan; szilyas@hotmail.com
[5] Faculty of Science, Engineering and Technology, Swinburne University of Technology, P.O. Box 218, Hawthorn, VIC 3122, Australia; salmansafi92@gmail.com
* Correspondence: tahir@awkum.edu.pk (M.T.); mahidursarker@ukm.edu.my (M.R.S.)

Abstract: This work reports on the synthesis of small molecular semiconductor 2-(1*H*-pyrrol-1-yl)-anthracene-9,10-dione (PAD) via wet chemical precipitation route method for its possible potential applications in sensors. Thin film characterization of the synthesized PAD is carried out by studying its surface morphology, bond dynamics, and optical properties. For studying sensing characteristics of the PAD, its 100 nm thick film is thermally deposited on pre-patterned silver (Ag) electrodes over glass substrate having ~45 µm inter-electrode gaps to prepare Ag/PAD/Ag sensor. The effects of humidity (%RH), temperature (T), and illumination of light (E_v) on the fabricated Ag/PAD/Ag sensor are studied by changing one of the three (%RH, T, and E_v) parameters at a time and measuring the corresponding variations in capacitance (C) and capacitive reactance (X) of the device. As C and X also depend on frequency, sensing properties of the Ag/PAD/Ag sensor are measured at two different frequencies (120 Hz and 1 kHz) to find the optimum sensitivity conditions. To investigate reproducibility and repeatability of Ag/PAD/Ag sensor, each measurement is taken several times and also hysteresis loops of %RH vs. C are plotted at 120 Hz and 1 kHz to find the percent errors in each cycle of measurements. The sensor is active to sense humidity, temperature, and illumination within a broad range, i.e., from 15–93%RH, 293–382 K, and 1500–20,000 lx, respectively. Other key parameters of the sensor i.e., the humidity response time (T_{Res}) and recovery time (T_{Rec}), are measured, which are 5 and 7 s, respectively, whereas for light sensing the values of T_{Res} and T_{Rec} are measured to be 3.8 and 2.6 s, respectively. The measured values of T_{Res} and T_{Rec} for the fabricated Ag/PAD/Ag sensor are shorter and better as compared to those of previously reported for similar kind of small molecular based sensors. The sensing properties of Ag/PAD/Ag device exhibit the potential of PAD for humidity, temperature, and light sensing applications.

Keywords: humidity sensor; temperature sensor; light sensor; organic semiconductor; pyrrol-anthracene-9,10-dione (PAD); response time and recovery time

check for updates

Citation: Zeb, M.; Tahir, M.; Muhammad, F.; Gul, Z.; Wahab, F.; Sarker, M.R.; Saad, M.H.M.; Alamgeer; Ali, S.; Ilyas, S.Z.; et al. Pyrrol-Anthracene: Synthesis, Characterization and Its Application as Active Material in Humidity, Temperature and Light Sensors. *Coatings* **2022**, *12*, 848. https://doi.org/10.3390/coatings12060848

Academic Editor: Ni Yang

Received: 19 May 2022
Accepted: 13 June 2022
Published: 17 June 2022

Publisher's Note: MDPI stays neutral with regard to jurisdictional claims in published maps and institutional affiliations.

Copyright: © 2022 by the authors. Licensee MDPI, Basel, Switzerland. This article is an open access article distributed under the terms and conditions of the Creative Commons Attribution (CC BY) license (https://creativecommons.org/licenses/by/4.0/).

1. Introduction

Sensors play a vital role in monitoring, quantifying and, hence, controlling various environmental parameters which are of significant interest for living-beings as well as for non-living things also. Mainly, humidity, temperature, and light illumination are some of

the environmental factors which have a direct impact on human-beings, plants, animals, and other fields of daily life such as food storage, medicines and drugs, etc. [1,2]. Due to unsuitable humidity, temperature, and light conditions, these are responsible for the degradation of medicines, rusting of iron, and the development of fungus on food items, leathers, woods, etc. Additionally, in order to properly develop some important organs of the living-beings, it is necessary to monitor, control, and maintain specific environmental parameters as in the case of various incubators being used for poultry, infants, and bacteriological purposes. For each of these incubators they require a specific level of humidity, temperature, oxygen, and light illumination. In commercial furnaces for tobacco plants processing, they also need to be processed at a particular humidity and temperature. Therefore, the strict observation, control, and maintaining of the essential environmental parameters is most significant. By these reasons, sensors have acquired remarkable consideration of researchers and scientists for its potential in various fields.

Previously, extensive research has been carried out on different kind of functional materials—inorganic and organic materials—for the fabrication of sensors. Mostly, the performance of inorganic materials has been reported to be better as compared to their organic counterparts. However, the high cost, brittleness, and tough processing of inorganic materials for device fabrication are their major disadvantages. On the other hand, organic materials offer mechanical flexibility, low-cost, easy, and simple processibility for device preparation. Sensors fabricated from organic semiconductors are found to be more useful, particularly for radiations [3–5], temperature [2,6], humidity [7], and gas [8] sensing. For this reason, recently, organic semiconductors have gotten significant attention from researchers and engineers for their unique electronic and optoelectronic properties. They can be categorized mainly in two classes, i.e., i. polymeric semiconductors and ii. small molecular semiconductors. Both of these types of materials possess the π-conjugation structure and delocalized π-bonds on the aromatic rings as well as the double bonds in the carbon chains that are responsible for their semiconducting behavior. A large number of organic semiconductors, including perylenes, prophyrins, phthalocyanine, polyfluorines, polyaniline, poly(p-phenylenediamine) etc. [1,5,9], have been employed as active materials for sensors applications. Among organic semiconductors, small molecules are of particular interest due their better chemical and thermal stability as compared to the polymers. Most of the small molecular semiconductors are insoluble in water and/or other organic solvents; hence, they are considered as good candidates for humidity sensing applications due to their hydrophobic nature.

However, the thrust is for synthesizing and exploring novel small molecular semiconductors with the desired characteristics that are suitable for sensing applications. Among small molecular materials, 2-(1*H*-pyrrol-1-yl)-anthracene-9,10-dione (PAD) is an n-type aromatic organic non-toxic semiconductor with a dark yellowish-brown color which is rich in pi-conjugated electrons [10–12]. Due to extraordinary properties of PAD, it has already established its applications in diverse fields such as pharmaceuticals as an antibacterial agent, agricultural products, catalytic hydrogenation process, and optoelectronic devices. However, an extensive investigated is needed to explore and study its sensing characteristics, since PAD possesses a hydrophobic nature and cannot be dissolved in water and/or other organic solvents which make it suitable for humidity sensing application. It has also good thermal, chemical, and mechanical stability, which is highly desirable and useful for temperature sensing [8,13,14]. It has strong and broad absorption in the ultraviolet-visible (UV–vis) spectrum from 260–540 nm, which is useful for illumination of light sensing UV–vis range.

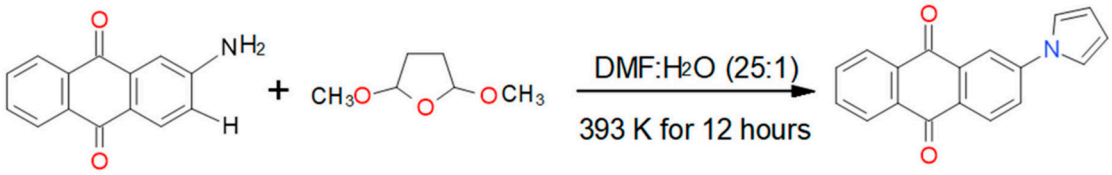
Herein, we report on the synthesis, thin film characterization and sensing properties of small molecular organic semiconductor PAD. For this purpose, PAD thin films are thermally deposited at high vacuum at ~10^{-6} mbar on quartz glass as well as on the pre-patterned Ag electrodes on glass substrate—where the inter-electrode gap between silver (Ag) electrodes is 45 μm—to form a surface type Ag/PAD/Ag sensor. The thin films developed on quartz glass are used for morphological, structural, and spectroscopic investigations. The

fabricated Ag/PAD/Ag device is characterized for exploring its humidity, temperature, and light sensing properties. Therefore, the capacitance and capacitive reactance of the device is measured as a function of humidity, temperature, and illumination of light.

2. Materials and Methods

2.1. Synthesis of PAD

The precursor materials, i.e., aminoanthracene-9,10-diones and 2,5-dimethoxytetrahydrofuran, were obtained from Sigma-Aldrich (Petaling Jaya, Malaysia). For the synthesis of PAD, 1.16 mL of 2,5-dimethoxytetrahydrofuran being 8.96 mmol was added to 4.48 mmol solution of 2-aminoanthracene-9,10-dione. Afterwards, the prepared solution was added to a mixture of dimethylformamide (DMF) and H_2O, having a 25:1 mL volume ratio. The reaction of the blend was initiated by using a hotplate and magnetic stirrer at a temperature of 393 K and 12 h. The product was then cooled and diluted in 150 mL of water. Then the precipitate was filtered, washed with de-ionized water, dried, and yellowish-brown powders were extracted with around 79% yield. The chemical reaction process is shown in Scheme 1.



Scheme 1. Synthesis reaction of PAD.

2.2. Sensor Fabrication

For device fabrication, a commercially available soda lime microscopic glass slide (20 mm × 20 mm) was employed as a substrate and Ag, obtained from Sigma Aldrich with >99% purity, was used as a top electrode. First of all, the glass substrate was cleaned with acetone and iso-propanol in each for 10 min using an ultrasonic bath and, subsequently, dried with the blow of dry nitrogen (N_2) gas. Shadow masking was used to form a ≈45 µm inter-electrode gap of between Ag electrodes via vacuum thermal evaporation, followed by the thermal deposition of a 100 nm thin layer of the synthesized PAD as an active sensing film on the pre-prepared Ag/glass electrodes. Thermal deposition was done by using an EDWARDS AUTO 306 vacuum thermal evaporator (Edwards, Crawley, UK) at a vacuum level of 1.5×10^{-6} mbar, whereas the growth rate is kept slower at 0.1 nm/s to form uniform films. All the film thicknesses are estimated from an in-situ thickness monitor (FTM5 quartz crystal, Edwards, Crawley, UK). The device is kept for heat treatment at 50 °C for 2 h to release mechanical stresses and strains present in the film. The schematic diagram of the fabricated sensors is shown in Figure 1.

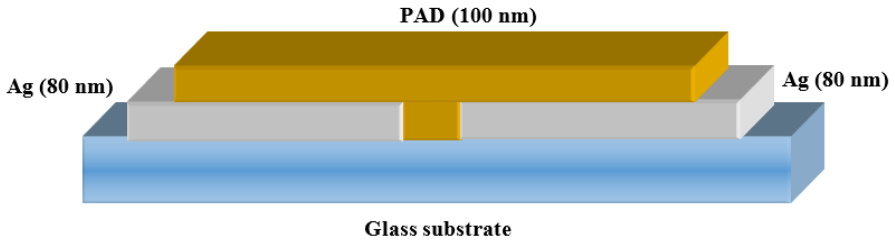


Figure 1. Schematic structure of Ag/PAD/Ag device.

2.3. PAD Thin Film and Sensor Characterization

Surface features of PAD thin films on quartz glass were studied by using AFM Nanoscope-IIIa SPM from Dimension TM 3100 Digital Instruments Veeco Metrology Group (Veeco, Cambridgeshire, UK) installed with a silicon cantilever having a resonance frequency, force constant, and tip radius of 160 kHz, 5 N/m, and <10 nm, respectively. For

ultraviolet-visible (UV–vis) absorption and Fourier transformed infrared (FTIR) spectra of PAD, Perkin-Elmer Lambda 1050 UV/vis/NIR and Perkin-Elmer Spectrum™ 3 FT-IR spectrometers (Perkin-Elmer, Buckinghamshire, UK) were used. A self-made humidity sensing setup was used to measure humidity sensing (i.e., change in capacitance and reactance of the Ag/PAD/Ag sensor as a function of humidity) which is shown in Figure 2a. The capacitive measurements as a function of relative humidity percent (%RH) of Ag/PAD/Ag device were performed by loading it in the airtight chamber wherein the relative humidity can be varied through the dry N_2 gas, introducing water vapors. As can be seen from Figure 2a, the Ag/PAD/Ag sensor is connected with a digital SERIE P-320 probed hygrometer for monitoring instantaneous %RH inside the chamber. The capacitance of the sensor at 1 kHz and 120 Hz was quantified with the help of an ESCORT ELC-133A LCR meter (ESZ, Eichenau, Germany). Furthermore, for temperature sensing, i.e., to measure capacitance and reactance of the fabricated sensor as a function of temperature, Karl Suss-PM5 probe station with a thermo chuck 'Alpha' series system, model TP 0315A-TS-2 of Temptronic Corporation, (Mansfield, MA, USA), was used. The temperature–capacitance measurements were conducted at normal ambient environment with 0%RH and under dark conditions. For illumination of light sensing of Ag/PAD/Ag device, as shown in Figure 2b, it was illuminated with continuous light from a source of a movable 25 W white LED such that the distance between the LED and sensor can be varied so that amount of illumination (illuminance) can be changed. Hence, capacitance and reactance of the device were studied as a function of illuminance.

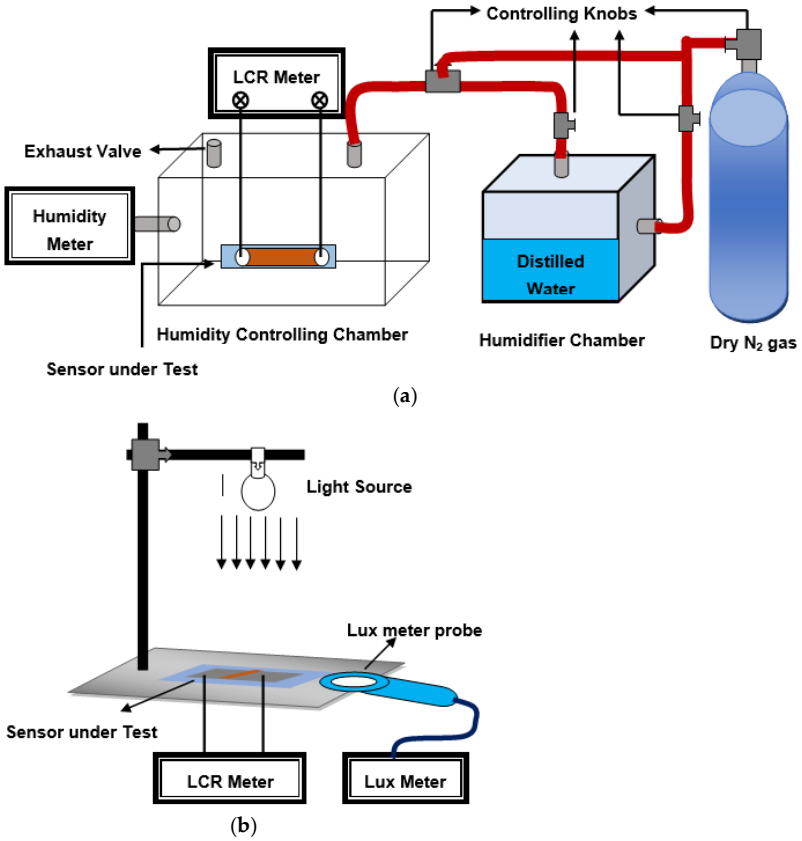


Figure 2. Schematic diagram of (**a**) humidity sensing setup and (**b**) light sensing setup.

3. Results and Discussion

Morphological features of the active layers have direct influence on the sensitivity of a sensor. Hence, it is essential to study the surface morphology of PAD films and understand the link with the performance of Ag/PAD/Ag surface type sensor. For this purpose, atomic force microscope (AFM) is used in non-contact mode at the surface's scan rate of 0.80 Hz to take image of PAD film. Three-dimensional (3-D) AFM micrographs of the PAD thin

films are shown in Figure 3a,b at 5 μm × 5 μm and 2 μm × 2 μm scales, respectively. The micrographs reveal particles' agglomeration in some regions andnon-uniformly distributed pores and interstitial spaces at the other regions [15–17]. Due to the non-uniform growth of PAD film during thermal deposition, these mosaics and islands are formed on the surface of the film, which can be clearly seen in Figure 3. This uneven surface features give rise to surface roughness which is measured as the average surface roughness (R_a) and is found to be 41 ± 5 nm. This porosity and surface roughness of the PAD films is greatly beneficial, especially for the humidity sensitivity, as they play a key role in adsorption and desorption of water molecules [14,18]. More adsorption and desorption of water droplets at the surface of PAD film result in significant change in dielectric constant and, hence, in the capacitance as well as capacitive reactance of the Ag/PAD/Ag sensor [19,20].

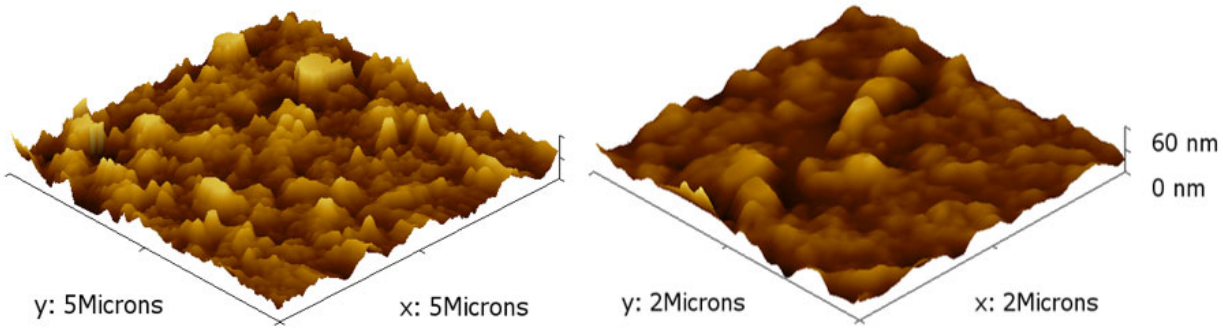


Figure 3. 3-D AFM micrographs of PAD thin film on quartz glass (**a**) on 5 μm and (**b**) 2 μm scale.

Figure 4 shows the UV–vis absorption curve of PAD which represents two prominent peaks within a broad spectrum ranging from near UV to visible region. The highest positions of peaks lie at 298 and 534 nm that correspond to the Soret or B-band and Q band, respectively. The B band is a characteristic transition of mobile electrons from the second π-π* transitions corresponding to the ground state (s_0) to the second exited state (s_2). Due to the large energy gap between these two states ($s_0 \rightarrow s_2$), B-band lies in the UV region. On the other hand, Q band is due to first π-π* transitions, i.e., from the ground state to the first excited state ($s_0 \rightarrow s_1$) of the aromatic ring present in the PAD. The Q-band corresponds to the visible region of the spectrum due to lower energy gap between $s_0 \rightarrow s_1$ transitions. The bandwidth of the Q-band for PAD is ranging from around of 450–600 nm, as shown in Figure 4. This suggests PAD to be sensitive to light within a broad spectrum at both UV and visible regions [20–22].

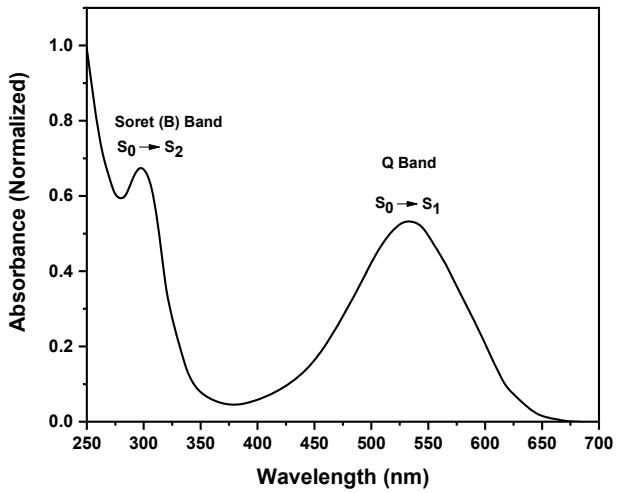


Figure 4. UV–vis absorption spectrum of PAD.

Figure 5 shows the FTIR spectrum of PAD plotted as wavenumber vs. percent transmittance (%T) in the bandwidth from 500 to 4000 cm^{-1}. The peaks lie at 605 cm^{-1}, 653 cm^{-1}, and from 709 cm^{-1} through 829 cm^{-1} to 933 cm^{-1} are attributed to the C-H stretching, C-H out of plane bending, and =C-H within aromatic ring out of plane bending vibration, respectively. Furthermore, the peaks at 1097, 1286, 1325 cm^{-1} correspond to C-N stretching whereas 1392, 1585, 1666, and 2362 cm^{-1} are due to the -CH_2 bending, C=C within aromatic ring, C=O and conjugated C=C stretching, respectively. Table 1 presents the overall FTIR bands, functional groups, and bond dynamics of PAD.

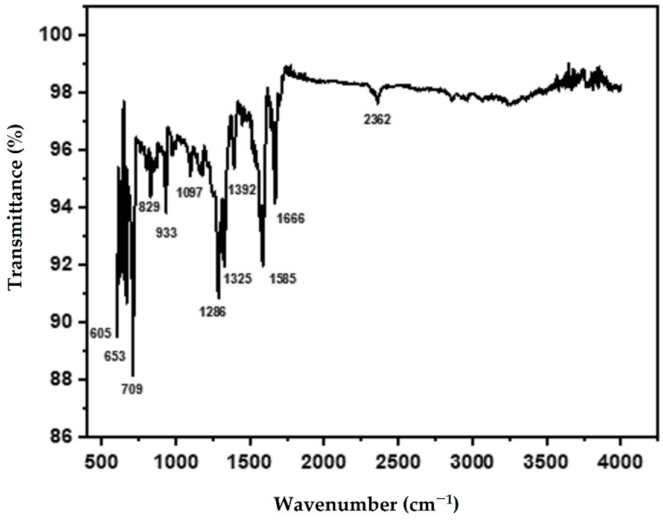


Figure 5. FTIR spectrum of PAD.

Table 1. Vibrational bond dynamics of PAD.

S. No.	Energy Bands (cm^{-1})	Bonds Nature/Dynamics
1	605	C-H stretching
2	653	C-H with alkenes out of plane bending
3	709	=C-H with aromatic out of plane bending
4	829	=C-H with aromatic out of plane bending
5	933	=C-H with aromatic out of plane bending
6	1097	C-N stretch
7	1286	C-N stretch
8	1325	C-N stretch
9	1392	-CH_2 bending
10	1585	C=C within aromatic ring
11	1666	C=O with amide
12	2362	C=C conjugated stretching

Humidity has great importance among the environmental parameters because of its consequences on the comfort of living-beings and industrial processes [23]. The relative humidity is defined as follows:

$$\%RH = \frac{\text{actual vapor density}}{\text{saturated vapor density}} \times 100\% \quad (1)$$

The operating frequency of capacitive type sensors impacts their sensing performance [24], and usually, it is suggested to use frequency higher than 100 Hz operating frequency for humidity sensors to diminish any interface-trapped charge carriers, which generate excess capacitance through polarization [25]. However, by applying lower operating frequencies better sensitivity can be achieved, but repeatability and stability will be significantly influenced [26]. Therefore, in the current work, we have applied operating frequencies higher than 100 Hz, i.e., 120 Hz and 1 kHz, as shown in Figure 6a.

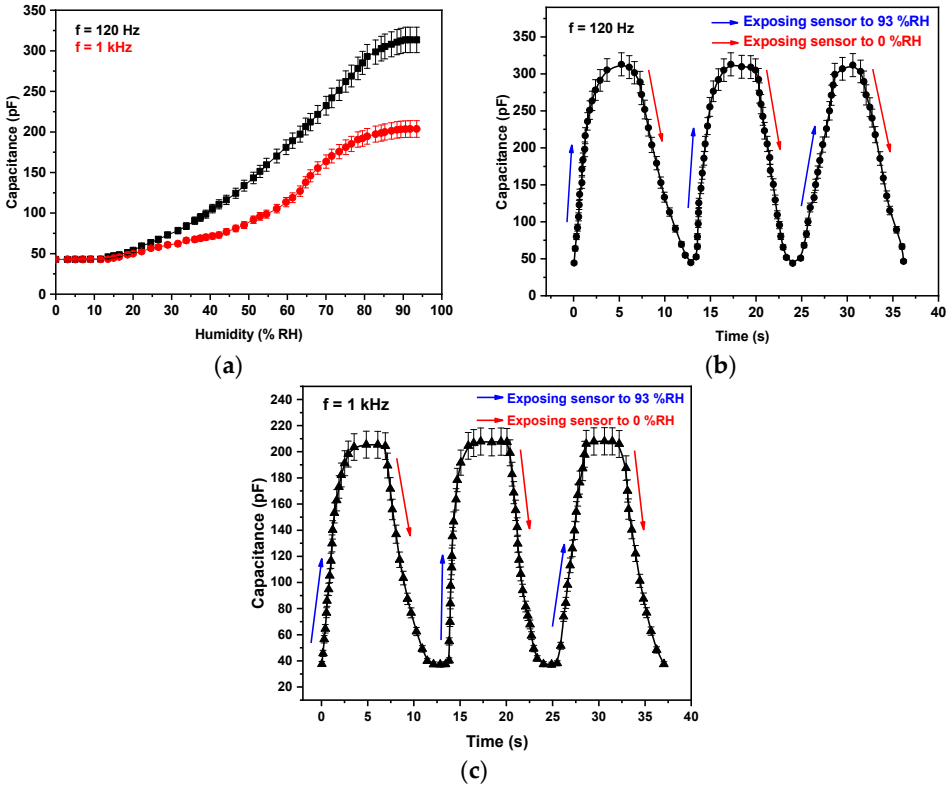


Figure 6. (**a**) Capacitance as a function of relative humidity (%RH) at 120 Hz and 1 kHz, (**b**) response/recovery-time curve at 120 Hz, and (**c**) response/recovery-time graph at 1 kHz for Ag/PAD/Ag sensor.

The capacitive humidity sensing response of the prepared Ag/PAD/Ag sensor at 120 Hz and 1 kHz within a broad range of 0–93%RH is shown in Figure 6a. The relative humidity was increased by 2%RH in each step and sustained for 5 min to let the sensor stabilize entirely. A significant increase in the sensor's capacitance was recorded as the humidity level was increased from 0%RH to 93%RH inside the test chamber. At lower humidity levels, i.e., from 0 to 20%RH, there is a modest rise in the sensor capacitance due to smaller quantities of adsorbed water vapors, which is not enough to significantly increase the dielectric constant of the active layer. A substantial increase happens in the sensor capacitance above 20%RH, which can be explained by the following expression, where the Ag/PAD/Ag device is assumed to behave as a capacitor:

$$C = \varepsilon_0 \varepsilon_r A/d \quad (2)$$

where ε_r is the relative dielectric constant of PAD, ε_0 is the permittivity of free space, A is the active PAD film area, and d is the spacing between the electrodes. Accumulation of more water vapors inside the test chamber causes more adsorption of water molecules in the voids and pores of the film surface, which upsurges ε_r of the sensing layer and, subsequently, gives rise to the sensor capacitance. As the dielectric constant of water (ε = 78) is significantly larger than that of the organic semiconducting materials (ε = 4–8), therefore, the sensor capacitance tends to increase as more water molecules are adsorbed onto the sensing layer [27]. The sensor shows a sensitivity of 3.46 pF/%RH and 1.94 pF/%RH at 120 Hz and 1 kHz, respectively, and more importantly the sensor is active within a broad range of humidity levels from 5%RH to 93%RH, which makes it a potential candidate for practical applications in those areas where both the low and high concentration of humidity detection is needed.

Response and recovery times are important parameters that are measured to evaluate the performance of a sensor for practical applications. The response time of a sensor is a

measure of how quickly the sensor responds to sense variations in its environment and to obtain the highest value, while the recovery time is a measure of time during which a sensor returns to its initial value by separating from the environmental variations. In Figure 6b,c, the response and recovery times of Ag/PAD/Ag sensor towards humidity variations are shown at 120 Hz and 1 kHz, respectively. At 120 Hz, the sensor shows an ultra-quick response (5.1 ± 0.2 s) when it is exposed to 93%RH and fast recovery (7.2 ± 0.2 s) by exposing it to 0%RH, whereas at 1 kHz, the average response and recovery times are measured to be 4.5 ± 0.2 s and 6.8 ± 0.2 s, respectively. These shorter response and recovery times make Ag/PAD/Ag sensor a suitable candidate for practical applications where quick detection of humidity is needed. Besides quick response and recovery times, the sensor also showed excellent recyclability, as shown in Figure 6b,c. The sensitivity of a humidity sensor can be measured by using the following relation.

$$S_H = \frac{C_{93} - C_{20}}{93 - 20} \left(pF/\%RH\right) \quad (3)$$

The humidity sensing mechanism can be defined by adsorption of water molecules on the surface of the sensing film and their effect on sensor capacitance. As water is polar in nature, the adsorption of a water molecule on the surface of film can be categorized into two phases, chemisorption and physisorption [28]. At low-humidity concentrations, water molecules chemisorb on the sensing layer. The water molecules in the chemisorption layer are not so mobile because water molecules are doubly bonded with the surface of the film. However, water molecules existing in physisorption layers are singly bonded, so water molecules can move freely and easily and can also be polarized easily [29]. The consecutive physisorption layers can be easily polarized due to the presence of singly bonded molecules. Thus, the relative permittivity and capacitance increase easily [30]. In high humid environments, successive multilayer adsorption of water molecules happens, which turns like a normal condensed liquid and affords an approving condition for the process of charge transportation resulting in Grotthuss chain reaction ($H_2O + H_3O^+ = H_3O^+ + H_2O$) [31]. In this situation, the electric field ionizes the water molecules, which produce hydronium ions (H_3O^+) as charge carriers, which produce protons ($H_3O^+ \rightarrow H_2O + H^+$) due to hydration. These protons need very low energy for hopping between adjacent water molecules; as a result, the ionic conductivity increases [32]. The schematic diagram of the proposed humidity sensing mechanism is shown in Figure 7 below.

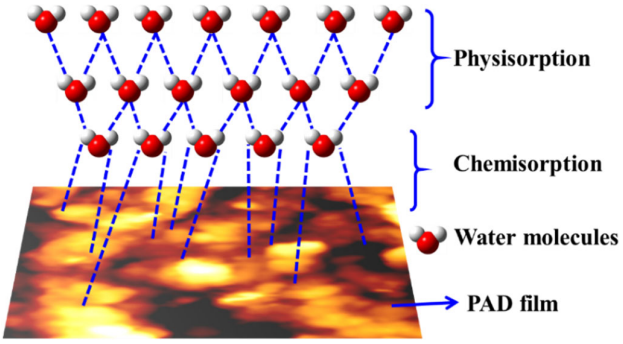


Figure 7. Schematic illustration of humidity sensing mechanism.

Hysteresis is an important feature of a humidity sensor, as it classifies its suitability for recurrent and practical use. The hysteresis curves of Ag/PAD/Ag sensor, recording the capacitance alongside the %RH level within 0 to 93%RH and contrariwise at both 120 Hz and 1 kHz, are shown in Figure 8a,b, respectively. The sensor narrow hysteresis loop at both operating frequencies validates exceptional repeatability and rapid adsorption and desorption rate of water molecules over the surface of the sensing film.

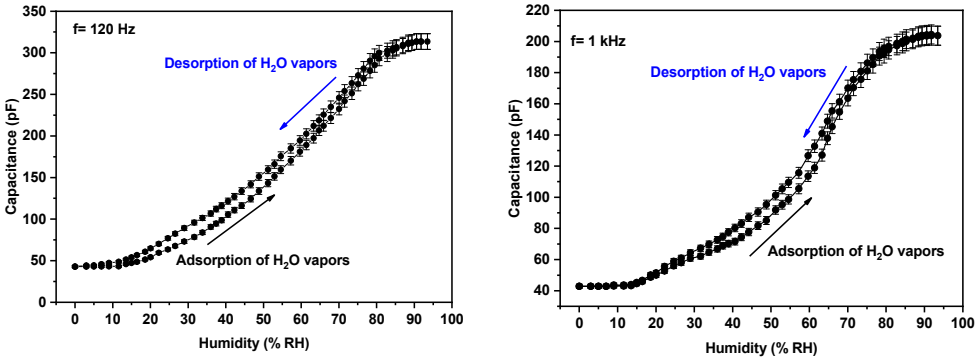


Figure 8. Hysteresis curves of Ag/PAD/Ag sensor at (**a**) 120 Hz and (**b**) 1 kHz.

In order to study the temperature sensing of Ag/PAD/Ag device, it is important to understand the temperature dependence on mobility and conduction of charge carriers of the PAD thin film. The increase in temperature (T) results in decrease of resistivity (ρ) of the PAD film, and can be linked according to the following equation:

$$\rho = \rho_0 \exp\left(\frac{E}{kT}\right) \tag{4}$$

where ρ is the resistivity of PAD film at absolute temperature T and E is the activation energy required for conduction of charge carriers, ρ_0 is the pre-exponential term, and k is the Boltzmann constant. Moreover, ρ and conductivity (σ) have inversely related to one another as given by:

$$\rho = \frac{1}{\sigma} \tag{5}$$

Consequently, decreases in the value of ρ give rise to increase the values of σ and lowers the resistance and/or reactance of the Ag/PAD/Ag device. Furthermore, the capacitance (C) and capacitive reactance (X) of the device at a given frequency (f) are inversely related to each other and given by the following equation;

$$C = \frac{1}{2\pi fX} \tag{6}$$

In line with Equations (4)–(6), the temperature sensing properties of Ag/PAD/Ag sensor are studied by variation in capacitance and reactance as a function of temperature. Figure 9a,b shows the temperature vs. capacitance and reactance curves at 120 Hz and 1 kHz operating frequencies within a temperature range of 293–382 K. It is clear that capacitance increases with the increase in temperature while opposite happens for the reactance. Hence, the increase in relative capacitance (C/C_0) of the Ag/PAD/Ag device is observed to increase 2.7 and 2.5 times at 120 Hz and 1 kHz, respectively. The effective capacitance (C_{eff}) of the sensor due to temperature response of the PAD active layer varies from 42.6–105 pF at 1 kHz and 42.9–115 pF at 120 Hz. Similarly, the decrease in relative reactance (X/X_0) of the Ag/PAD/Ag device is found to be increased by 0.40 and 2.4 times at 1 kHz and 120 Hz, respectively. The effective reactance (X_{eff}) of Ag/PAD/Ag sensor varies within 1.2–3.0 MΩ at 1 kHz, while 1.2–2.8 MΩ at 120 Hz. The Ag/PAD/Ag sensor showed high sensitivity towards temperature besides humidity, which makes it a suitable candidate for multifunctional sensor. The temperature sensing mechanism for Ag/PAD/Ag based sensor can be explained from the effect of temperature on conductivity and mobility of PAD thin film, as described from Equations (4)–(6). By increasing the temperature of the sensor, the resistivity of the PAD film decreases, and as a result conductivity and capacitance increases [33].

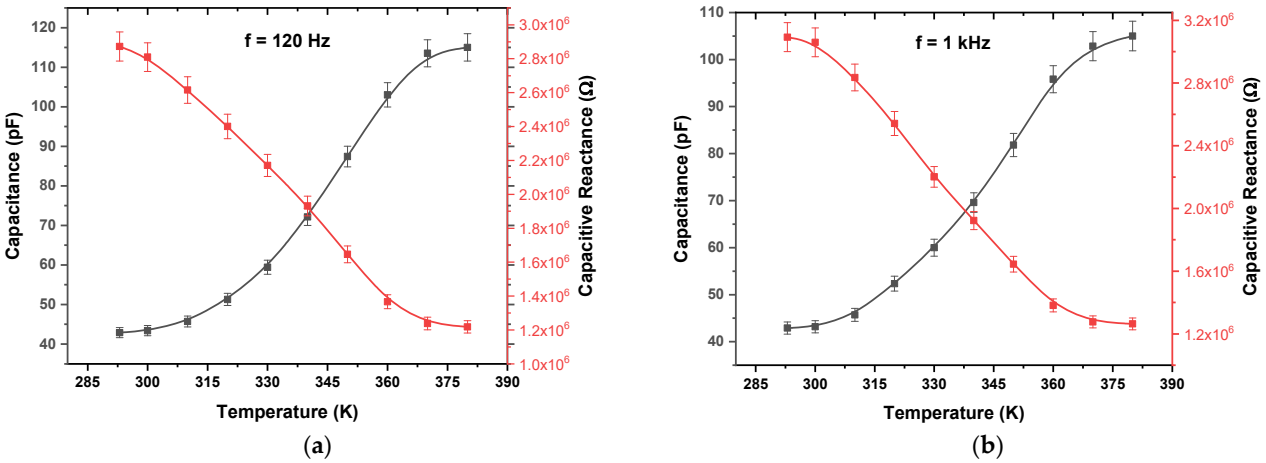


Figure 9. Effect of temperature on capacitance and reactance of Ag/PAD/Ag sensor at (**a**) 120 Hz and (**b**) 1 kHz.

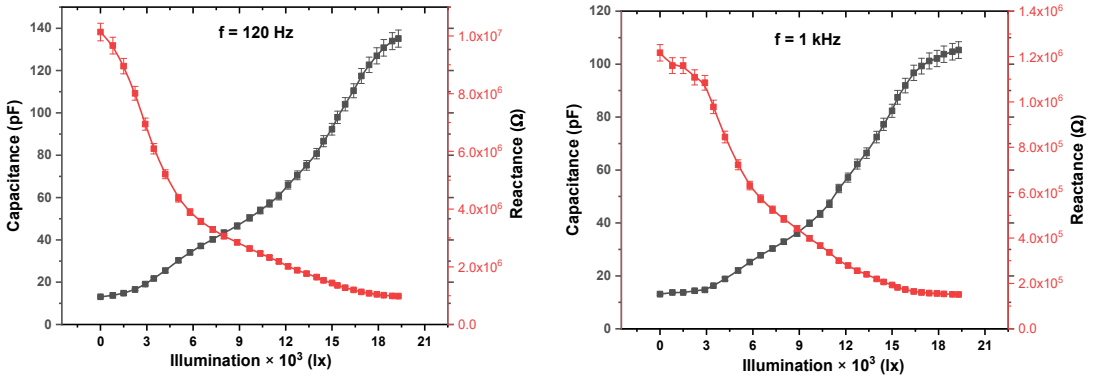
The temperature sensitivity of Ag/PAD/Ag device can be calculated as follows:

$$S_T = \frac{C_{382} - C_{293}}{382 - 293} (pF/K) \quad (7)$$

where S_T is the temperature sensitivity of the sensor, C_{293} is the capacitance at a temperature of 293 K, and C_{382} is the capacitance at 382 K. At 1 kHz and 120 Hz, the temperature sensitivity of the Ag/PAD/Ag device in the given temperature range (293–382 K) is calculated to be 0.73 pF/K and 0.82, respectively.

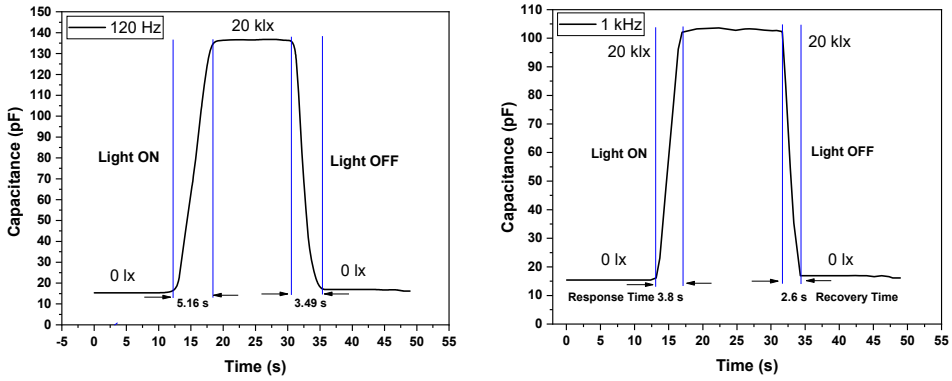
To furthermore push the practicality of Ag/PAD/Ag prototype sensor, we also investigated its light sensing properties. The illumination against capacitance and reactance relationship of the sensor at room temperature is shown in Figure 10. A luminescent light has been utilized to expose the sensor systematically from '0' lx (dark condition) to 20,000 lx (illumination). The amount of illumination was altered by varying the gap between Ag/PAD/Ag sensor and the light source. Primarily, the light was illuminated from 60 cm distance above the sensor. The distance was altered in a fixed step size of 3 cm with an average exposure time of 5 s to get the values stable. It is clear from Figure 10a,b that the capacitance increases and reactance decreases sharply as the amount incident light exceeds 1500 lx and it increases quickly and continuously until the exposure of 18,000 lx, and then above 18,000 lx the sensor goes into saturation. The capacitance of the sensor increases almost 10.3 times upon exposure to 20,000 lx at 120 Hz. The value of C_{eff} due to illumination of light of the Ag/PAD/Ag sensor changes from 13.0–135.1 pF at 120 Hz and 13.0–105.3 pF at 1 kHz, whereas the value of X_{eff} of the sensor due to light lies in the range of 0.9–10.1 MΩ at 120 Hz and 0.1–1.2 MΩ at 1 kHz. Charge carrier concentration increases with the increase in the amount of illumination, which in turn increases the polarizability because of transfer of charge carriers and, consequently, increases the capacitance and decreases the reactance of the sensor [14].

Furthermore, the response and recovery times of the Ag/PAD/Ag light sensor is also investigated by exposing the sensor to illumination within the range of 0–20,000 lx at 120 Hz and 1 kHz as shown in Figure 11a,b, respectively. At 120 Hz, the sensor exhibited the response and recovery times to be 5.1 ± 0.2 s and 3.4 ± 0.2 s, respectively, whereas at 1 kHz the response time is measured to be 3.8 ± 0.2 s and recovery time as 2.6 ± 0.2 s. At 1 kHz, the Ag/PAD/Ag sensor showed ultrafast response towards illumination of light and shorter recovery time upon switching off the light. The higher light sensitivity and ultrafast response, as well as recovery time of the Ag/PAD/Ag sensor, make it a promising candidate to be used in photodetectors, where the quick detection of light is desirable.



(**a**) (**b**)

Figure 10. Capacitance and reactance–light relationships of Ag/PAD/Ag sensor at (**a**) 120 Hz and (**b**) 1 kHz.



(**a**) (**b**)

Figure 11. Response/recovery curve of Ag/PAD/Ag light sensor at (**a**) 120 Hz and (**b**) 1 kHz.

The Ag/PAD/Ag prototype-multifunctional sensor has been investigated for humidity, temperature, and light sensing applications, and has shown a promising response towards all the targeted parameters. All types (humidity, temperature, and light) of sensors can be prepared on a single substrate, which would certainly minimize the overall cost, although the interaction of various effects may be diminished by having separate casing and designs with suitable window for each sensor. Table 2 presents the comparison of various sensors' parameters of Ag/PAD/Ag device with those of reported in the literature. It can be seen that Ag/PAD/Ag device shows relatively better sensing performance in terms of the broader sensitive ranges and better values of sensitivities for humidity, temperature, as well as light and shorter response and recovery times with better reproducibility of results.

Table 2. Comparison of present work with literature.

Device	Relative Humidity		Temperature		Illumination	References
	Sensitivity (pF/%RH)	Range (%RH)	Sensitivity (pF/K)	Range (K)	Sensitive Range (lx)	
Ag/CuTIPP/Ag	3.40	44–92	0.2	298–423	-	[34]
Au/AAq/Au	0.40	40–88	0.87	295–388	-	[33]
Ag/Mo/Ag	3.10	35–95	0.2	333–473	-	[35]
Au/N-BuHHPDI/Au	20.00	60–90	0.05	400–460	7000–25,000	[14]
Al/VoPc/Pt	2.53	60–90	-	-	-	[36]
Ag/IESM/Ag	0.42	20–90	-	-	-	[37]
Al/ZnPc/Al	1.03	20–95	-	-	-	[38]
Ag/PAD/Ag	3.46	15–93	0.82	293–382	1500–20,000	Present Work

The schematic illustration of complete and equivalent circuits for the Ag/PAD/Ag sensor is shown in Figure 12a,b, respectively. In Figure 12a, X_a and X_g represent the reactance due to air and glass substrate, respectively, while X_{eff} denotes the reactance due to humidity, temperature, and light illumination. Similarly, C_a and C_g are capacitances due to air and glass substrate, respectively, whereas C_{eff} is the effective capacitance due to humidity, temperature, and illumination of light. The effect of air and glass substrate on the reactance and capacitance is constant and does not vary reasonably with the variations in humidity, temperature, and illumination of light. Hence, it is the active PAD layer that dominantly changes its capacitance and reactance as a function of humidity, temperature, and light. Therefore, in Figure 12b, an equivalent circuit diagram of the effective parameters (X_{eff}, C_{eff}) is illustrated that takes into account the reactance and capacitance of the PAD layer only.

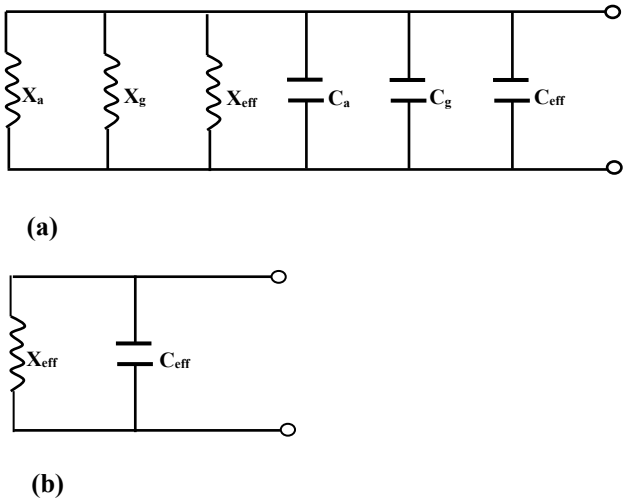


Figure 12. Equivalent circuit diagram of Ag/PAD/Ag sensor (**a**) detailed (**b**) effective.

4. Conclusions

In this work, a novel small organic molecular semiconductor PAD is successfully synthesized and characterized for its potential in humidity, temperature, and light sensing applications. The PAD thin films are also studied for their morphological and spectroscopic properties. The morphology revealed good film formation via vacuum thermal deposition, with some non-uniformity and roughness at the surface of the layer. Furthermore, UV–vis results of PAD exhibited broad absorption spectrum with a peak at 298 nm in UV and another peak at 534 nm, having a wide range of 450–600 nm in the visible region. The molecular structure, functional groups, and bond dynamics analyzed via FTIR confirmed the successful synthesis of PAD. The sensing characteristics of Ag/PAD/Ag device showed better performance towards humidity, temperature, and light sensing within a broad range of 15–93%RH, 293–382 K, and 1550–18,000 lx, respectively. The response and recovery times for humidity sensing were found to be 5 and 7 s, respectively. For illumination of light sensing, the response time was 3.8 s while the recovery time was 2.6 s. Due to the broader sensitive range, good chemical and thermal stability, as well as shorter response/recovery times of PAD based sensor, this study suggests the potential application of PAD as a good candidate for sensors to monitor environmental conditions.

Author Contributions: Conceptualization, M.T. and M.Z.; methodology, M.T. and F.M.; software, M.T., S.A. (Shabina Ali), and Z.G.; validation F.M., M.R.S., Z.G., and M.T.; formal analysis, M.T., S.A. (Shabina Ali), and M.R.S.; investigation, M.T., M.Z., and A.; resources, M.T., F.W., and M.Z.; data curation, M.T., S.Z.I., and M.R.S.; writing—M.T., S.A. (Salman Ali), and M.Z.; writing—review and editing, M.T., F.W., S.Z.I., M.R.S., and M.H.M.S.; supervision, M.T.; project administration, M.T.; funding acquisition, M.R.S. and M.H.M.S. All authors have read and agreed to the published version of the manuscript.

Funding: Universiti Kebangsaan Malaysia (UKM) for funding the research under Grant Code GGPM-2021-050 and PP-IIR4-2022.

Institutional Review Board Statement: Not applicable.

Informed Consent Statement: Not applicable.

Data Availability Statement: Not applicable.

Acknowledgments: All the authors are grateful to the Semiconductor Physics and Devices Laboratory, Abdul Wali Khan University Mardan, Pakistan, and the Higher Education Commission (HEC) of Pakistan, for providing the research facilities and Project. No.10170/KPK/NRPU/R&D/HEC/2017.

Conflicts of Interest: The authors declare no conflict of interest.

References

1. Köse, R. An evaluation of wind energy potential as a power generation source in Kütahya, Turkey. *Energy Convers. Manag.* **2004**, *45*, 1631–1641. [CrossRef]
2. Liguras, D.K.; Kondarides, D.I.; Verykios, X.E. Production of hydrogen for fuel cells by steam reforming of ethanol over supported noble metal catalysts. *Appl. Catal. B Environ.* **2003**, *43*, 345–354. [CrossRef]
3. Zeb, M.; Tahir, M.; Muhammad, F.; Mohd Said, S.; Mohd Sabri, M.F.; Sarker, M.R.; Hamid Md Ali, S.; Wahab, F. Amplified spontaneous emission and optical gain in organic single crystal quinquethiophene. *Crystals* **2019**, *9*, 609. [CrossRef]
4. Suri, K.; Annapoorni, S.; Sarkar, A.K.; Tandon, R.P. Gas and humidity sensors based on iron oxide–polypyrrole nanocomposites. *Sensors Actuators B Chem.* **2002**, *81*, 277–282. [CrossRef]
5. Deb, S.K. Opportunities and challenges in science and technology of WO_3 for electrochromic and related applications. *Sol. Energy Mater. Sol. Cells* **2008**, *92*, 245–258. [CrossRef]
6. Yan, H.; Chen, Z.; Zheng, Y.; Newman, C.; Quinn, J.R.; Dötz, F.; Kastler, M.; Facchetti, A. A high-mobility electron-transporting polymer for printed transistors. *Nature* **2009**, *457*, 679–686. [CrossRef]
7. Schriever, C.; Barbatti, M.; Stock, K.; Aquino, A.J.A.; Tunega, D.; Lochbrunner, S.; Riedle, E.; de Vivie-Riedle, R.; Lischka, H. The interplay of skeletal deformations and ultrafast excited-state intramolecular proton transfer: Experimental and theoretical investigation of 10-hydroxybenzo[h]quinoline. *Chem. Phys.* **2008**, *347*, 446–461. [CrossRef]
8. Freeman, C.G.; Litjens, R.A.J.; Quickenden, T.I. Visible and near-ultraviolet absorption spectrum of liquid water. *Appl. Opt. Vol.* **1999**, *38*, 1216–1223. [CrossRef]
9. Tahir, M.; Ilyas, M.; Aziz, F.; Sarker, M.R.; Zeb, M.; Ibrahim, M.A.; Mohamed, R. Fabrication and microelectronic properties of hybrid organic–inorganic (poly(9,9, dioctylfluorene)/p-Si) heterojunction for electronic applications. *Appl. Sci.* **2020**, *10*, 7974. [CrossRef]
10. Koh, J.H.; Sorge, E.; Wen, T.C.; Shetty, D.K. Thermal expansion behaviors of yttrium tungstates in the WO_3-Y_2O_3 system. *Ceram. Int.* **2013**, *39*, 8421–8427. [CrossRef]
11. Hara, M.; Kondo, T.; Komoda, M.; Ikeda, S.; Kondo, J.N.; Domen, K.; Hara, M.; Shinohara, K.; Tanaka, A. Cu_2O as a photocatalyst for overall water splitting under visible light irradiation. *Chem. Commun.* **1998**, *3*, 357–358. [CrossRef]
12. Muhammad, F.; Tahir, M.; Zeb, M.; Kalasad, M.N.; Mohd Said, S.; Sarker, M.R.; Sabri, M.F.M.; Ali, S.H.M. Synergistic enhancement in the microelectronic properties of poly-(dioctylfluorene) based Schottky devices by CdSe quantum dots. *Sci. Rep.* **2020**, *10*, 1–13. [CrossRef]
13. Le Houx, N.; Pourroy, G.; Camerel, F.; Comet, M.; Spitzer, D. WO_3nanoparticles in the 5−30 nm range by solvothermal synthesis under microwave or resistive heating. *J. Phys. Chem. C* **2010**, *114*, 155–161. [CrossRef]
14. Tahir, M.; Sayyad, M.H.; Clark, J.; Wahab, F.; Aziz, F.; Shahid, M.; Munawar, M.A.; Chaudry, J.A. Humidity, light and temperature dependent characteristics of Au/N-BuHHPDI/Au surface type multifunctional sensor. *Sens. Actuators B Chem.* **2014**, *192*, 565–571. [CrossRef]
15. Chen, Z.; Zhao, D.; Ma, R.; Zhang, X.; Rao, J.; Yin, Y.; Wang, X.; Yi, F. Flexible temperature sensors based on carbon nanomaterials. *J. Mater. Chem. B* **2021**, *9*, 1941–1964. [CrossRef]
16. Khan, D.N.; Sayyad, M.H.; Tahir, M.; Wahab, F.; Yaseen, M.; Ali, M.; Munawar, M.A. The sensing of humidity by surface-type ag/formyl-tippcu(ii)/ag sensor for environmental monitoring. *Surf. Rev. Lett.* **2014**, *21*, 1450048. [CrossRef]
17. Muhammad, F.; Tahir, M.; Zeb, M.; Wahab, F.; Kalasad, M.N.; Khan, D.N.; Karimov, K.S. Cadmium selenide quantum dots: Synthesis, characterization and their humidity and temperature sensing properties with poly-(dioctylfluorene). *Sens. Actuators B Chem.* **2019**, *285*, 504–512. [CrossRef]
18. Tahir, M.; Sayyad, M.H.; Wahab, F.; Aziz, F.; Shahid, M.; Munawar, M.A. Perylene diimide: Synthesis, fabrication and temperature dependent electrical characterization of heterojunction with p-silicon. *Phys. B Condens. Matter* **2013**, *426*, 6–12. [CrossRef]
19. Wajid, A.; Tahir, M.; Arif; Uddin, S.I.; Wahab, F. Humidity and temperature dependent characteristics of Ag/$SnNcCl_2$/Ag surface type multifunctional sensor. *Surf. Rev. Lett.* **2019**, *27*, 1950148. [CrossRef]
20. Zou, Y.; Clark, J.D.; May, A.A. A systematic investigation on the effects of temperature and relative humidity on the performance of eight low-cost particle sensors and devices. *J. Aerosol. Sci.* **2021**, *152*, 105715. [CrossRef]

21. Speranza, G. Carbon nanomaterials: Synthesis, functionalization and sensing applications. *Nanomaterials* **2021**, *11*, 967. [CrossRef] [PubMed]
22. Tahir, M.; Zeb, M.; Alamgeer; Hussain, S.; Sarker, M.R.; Khan, D.N.; Wahab, F.; Ali, S.H.M. Cuprous oxide nanoparticles: Synthesis, characterization, and their application for enhancing the humidity-sensing properties of poly(dioctylfluorene). *Polymers* **2022**, *14*, 1503. [CrossRef] [PubMed]
23. Meng, J.; Ma, J.N.; Li, J.; Yan, H.; Meng, F. Humidity sensing and temperature response performance of polymer gel cold-spliced optical fiber Fabry-Perot interferometer. *Opt. Fiber Technol.* **2022**, *68*, 102823. [CrossRef]
24. Ali, S.; Jameel, M.A.; Harrison, C.J.; Gupta, A.; Shafiei, M.; Langford, S.J. Nanoporous naphthalene diimide surface enhances humidity and ammonia sensing at room temperature. *Sens. ActuatorsB Chem.* **2022**, *351*, 130972. [CrossRef]
25. Zhang, Y.; Wu, J.; Zhang, Y.; Guo, W.; Ruan, S. Characterization and humidity sensing properties of the sensor based on $Na_2Ti_3O_7$ nanotubes. *J. Nanosci. Nanotechnol.* **2014**, *14*, 4303–4307. [CrossRef]
26. Al-Sehemi, A.G.; Al-Assiri, M.S.; Kalam, A.; Zafar, Q.; Azmer, M.I.; Sulaiman, K.; Ahmad, Z. Sensing performance optimization by tuning surface morphology of organic (D-π-A) dye based humidity sensor. *Sens. Actuators B Chem.* **2016**, *231*, 30–37. [CrossRef]
27. Najeeb, M.A.; Ahmad, Z.; Shakoor, R.A. Organic thin-film capacitive and resistive humidity sensors: A focus review. *Adv. Mater. Interfaces* **2018**, *5*, 1800969. [CrossRef]
28. Ali, S.; Jameel, M.A.; Gupta, A.; Langford, S.J.; Shafiei, M. Capacitive humidity sensing performance of naphthalene diimide derivatives at ambient temperature. *Synth. Met.* **2021**, *275*, 116739. [CrossRef]
29. Gu, L.; Zheng, K.; Zhou, Y.; Li, J.; Mo, X.; Patzke, G.R.; Chen, G. Humidity sensors based on ZnO/TiO_2 core/shell nanorod arrays with enhanced sensitivity. *Sens. Actuators B Chem.* **2011**, *159*, 1–7. [CrossRef]
30. Li, L.Y.; Dong, Y.F.; Jiang, W.F.; Ji, H.F.; Li, X.J. High-performance capacitive humidity sensor based on silicon nanoporous pillar array. *Thin Solid Films* **2008**, *517*, 948–951. [CrossRef]
31. Chen, Z.; Lu, C. Humidity sensors: A review of materials and mechanisms. *Sens. Lett.* **2005**, *3*, 274–295. [CrossRef]
32. Ali, S.; Jameel, M.A.; Harrison, C.J.; Gupta, A.; Evans, R.A.; Shafiei, M.; Langford, S.J. Enhanced capacitive humidity sensing performance at room temperature via hydrogen bonding of cyanopyridone-based oligothiophene donor. *Chemosensors* **2021**, *9*, 320. [CrossRef]
33. Ali, S.; Tahir, M.; Mehboob, N.; Wahab, F.; Langford, S.J.; Said, S.M.; Sarker, M.R.; Julai, S.; Ali, S.H.M. Amino anthraquinone: Synthesis, characterization, and its application as an active material in environmental sensors. *Materials* **2020**, *13*, 960. [CrossRef] [PubMed]
34. Saleem, M.; Sayyad, M.H.; Karimov, K.S.; Yaseen, M.; Ali, M. Cu(II) 5,10,15,20-tetrakis(4′-isopropylphenyl) porphyrin based surface-type resistive-capacitive multifunctional sensor. *Sens. Actuators B Chem.* **2009**, *137*, 442–446. [CrossRef]
35. Tahir, M.; Hassan Sayyad, M.; Wahab, F.; Ahmad Khalid, F.; Aziz, F.; Naeem, S.; Naeem Khalid, M. Enhancement in the sensing properties of methyl orange thin film by TiO_2 nanoparticles. *Int. J. Mod. Phys. B* **2014**, *28*, 1450032. [CrossRef]
36. Aziz, F.; Sayyad, M.H.; Sulaiman, K.; Majlis, B.H.; Karimov, K.S.; Ahmad, Z.; Sugandi, G. Corrigendum: Influence of humidity conditions on the capacitive and resistive response of an Al/VOPc/Pt co-planar humidity sensor. *Meas. Sci. Technol.* **2012**, *23*, 069501. [CrossRef]
37. Khan, M.U.; Hassan, G.; Bae, J. Bio-compatible organic humidity sensor based on natural inner egg shell membrane with multilayer crosslinked fiber structure. *Sci. Rep.* **2019**, *9*, 5824. [CrossRef]
38. Mohamed Safian, N.A.; Anuar, A.; Omar, A.Z.; Bawazeer, T.M.; Alsenany, N.; Alsoufi, M.S.; Supangat, A.; Roslan, N.A. Enhanced sensitivity of zinc phthalocyanine-based microporous humidity sensors by varying size of electrode gaps. *Sens. Actuators B Chem.* **2021**, *343*, 130158. [CrossRef]